Conceptual Design Report: KATRIN with TRISTAN modules

TRISTAN group

The Karlsruhe Tritium Neutrino (KATRIN) experiment is designed to measure the absolute neutrino mass scale with a sensitivity of 0.2 eV (90% CL) based on a high-precision measurement of the tritium β-decay spectrum, close to its endpoint. The KATRIN experiment holds the world leading limit on the neutrino mass of $m_\nu < 0.8\,\mathrm{eV}$ and is therefore the first experiment to break the sub-eV sensitivity on a direct neutrino-mass measurement [1]. Its unprecedented tritium source luminosity and spectroscopic quality makes it a unique instrument to also search for physics beyond the Standard Model (BSM). Most notably, a keV-scale sterile neutrino would manifest with a characteristic signature several keV away from the endpoint. In order to extend the energy region of interest of KATRIN a novel detector and read-out system is necessary. To handle exceedingly high rates of up to 10^8 electrons per second, and provide excellent energy resolution (300 eV @ 20 keV) a focal plane array with more than 1000 Silicon Drift Detector (SDD) pixels is foreseen.

CONTENTS

I. SCIENCE PROGRAM

A. keV-scale sterile neutrino search

Sterile neutrinos are a well-motivated extension of the Standard Model (SM) of Particle Physics. Since the discovery of neutrino oscillation, which proofs that neutrinos have a mass, the existence of right-handed partners to the known left-handed neutrinos is a common assumption. A far-reaching consequence of the introduction of right-handed neutrinos, is the possible existence of new neutrino mass eigenstates. The corresponding new particles can have an arbitrary mass, and only interact gravitationally or via their mixing with the active SM neutrinos. Because of this property these postulated particles are also known as sterile neutrinos.

Sterile neutrinos with a mass in the kilo-electron-volt (keV) regime are promising Dark Matter candidates [2–4]. Due to their mass-scale and production mechanism, they can act as Warm Dark Matter, which could mitigate tensions between cosmological observations and predictions of purely Cold Dark Matter scenarios [5, 6].

A promising way to search for sterile neutrinos in the keV mass range is via the kinematics of β-decay [7–10]. For β-electron energies significantly below the kinematic endpoint, the decay into the heavy sterile neutrino along-side with the β-electron, becomes energetically accessible. The emission of a sterile neutrino would lead to an additional decay branch, with a maximal energy $E = E_0 - m_\mathrm{s}$ reduced by the sterile neutrino's mass m_s and a magnitude governed by the mixing amplitude $\sin^2\theta$ of the sterile neutrino with the active SM electron neutrino. The superposition of both spectra leads to a characteristic kink-like signature, as can be seen in figure 1.

The main challenge of a search for Dark Matter sterile neutrinos in β-decays, is the stringent limit of the order of $\sin^2\theta < 10^{-7}$ on their mixing amplitude based on astrophysical and cosmological observations [11–13]. Sterile neutrino Dark Matter decays (with a very long half-live) into active SM neutrinos and photons. Assuming that the whole Dark Matter content of the Universe would be exclusively composed of sterile neutrinos, the non-

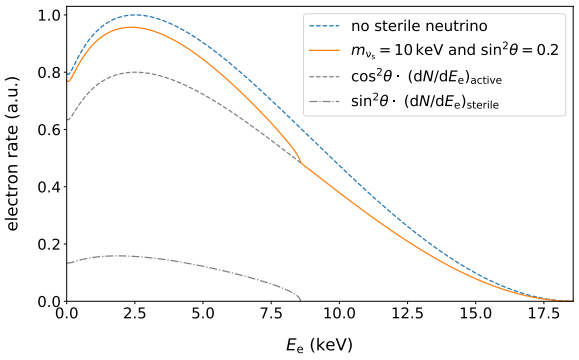

Figure 1: Imprint of a sterile neutrino with a mass of $m_s = 10\,\mathrm{keV}$ and an unphysically large mixing amplitude of $\sin^2\theta = 0.2$ on the tritium β-decay spectrum. The grey dash-dotted line depicts the decay branch into a sterile neutrino, the grey dashed line shows the regular decay branch into an active SM neutrino. The solid orange line is the resulting superposition of the two spectra, with the typically kink-like signature. As a comparison, the blue dashed line shows a spectrum without a sterile neutrino.

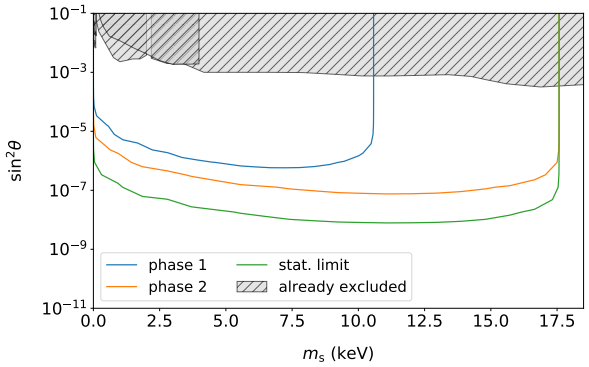

Figure 2: Sensitivity of KATRIN to keV-scale sterile neutrinos in different scenarios. The statistical limit is reached with a total statistics of 10^{18} electrons over the full energy range. This would correspond to a measurement time of 3 years at the full KATRIN source strength. In Phase-1 and Phase-2 a reduced source activity and a reduced analysis window (Phase-1) are assumed, in order to reduce the rate at the detector and systematic uncertainties. The individual settings of the different operation modes are listed in table I.

observation of a corresponding x-ray signal of the sterile neutrino decay can be translated in a strong bound on the parameter. Moreover, too large mixing amplitudes would lead to an overproduction of sterile neutrinos in the early universe exceeding today's total amount of Dark Matter.

These indirect observations provide valuable insights on possible new constituents of the universe, they are however model-dependent. For example, a recent publication [14] describes an alternative cosmological scenario where a large signal in β-decays would be possible, without violating the current x-ray limits. The advantage of a laboratory-based experiment is that no assumption on the underlying cosmological model, the production mechanism or the abundance and distribution of the particle in the cosmos have to be made.

The KATRIN experiment, equipped with the TRISTAN detector, has the potential to search for the signal of keV-scale sterile neutrinos. With 1-year of KATRIN operation at full source strength, a statistical sensitivity of the order of $\sin^2\theta = 10^{-8}$ could be reached. It is however extremely challenging to control systematic uncertainties at this level. Therefore, the targeted design sensitivity is $\sin^2\theta = 10^{-6}$, which would surpass the sensitivity of previous laboratory-based searches and reach a region of cosmological interest. Table I shows different measurement scenarios, using the KATRIN experiment and a TRISTAN detector to search for sterile neutrinos. The corresponding statistical sensitivity of the different stages of operation are shown in figure 2.

Table I: Possible setting for Phase-1 and Phase-2.

	Phase-1	Phase-2
Total statistics	$2 \cdot 10^{14}$	$1 \cdot 10^{16}$
Measurement time	0.5 years	1 years
Column density	0.3%	2%
qU range	$8 - 18\,\mathrm{keV}$	full range
Active pixels	1000	3500
Total rate	12.5 Mcps	300.0 Mcps
Rate per pixel	12.5 kcps	90.0 kcps

B. Spectral endpoint measurement

A key feature of the new detector system is its excellent energy resolution of 300 eV FWHM at 20 keV for electrons, which could advance the spectral measurement close to the endpoint. The improved energy resolution with respect to the current KATRIN focal plane detector would allow to reduce the Region of Interest (ROI) and thereby the detector-related background. In addition, the superior energy resolution can help to better discriminate the spectrometer-related background from the signal. This is possible in the new electromagnetic field setting of the KATRIN main spectrometer, where the analyzing plane is shifted significantly towards the detector, leading to significantly different starting energies for the background electrons.

C. Other new physics searches

Besides the search for keV-scale sterile neutrino and the benefits for the KATRIN neutrino mass determination, other signals of new physics could be detectable in a high-precision measurement of the tritium β-spectrum. The perspective of performing such measurement with KATRIN has triggered various publication where possible BSM signatures in β-decays are being discussed. These include the proposal to search for the signal of the emission of new light bosons [15], exotic charged current interactions [16], extra dimensional sterile neutrinos [17], and right-handed currents [18].

II. SEARCH FOR STERILE NEUTRINOS WITH KATRIN

The search for keV-scale sterile neutrinos with the KATRIN experiment involves several challenges, which are related to the location and size of the signature. The kink-like distortion of the spectrum, caused by the emission of a sterile neutrino, could be located several keV away from the endpoint and the height of the signal directly scales with the active-to-sterile mixing amplitude $\sin^2\theta$, which is expected to be very small ($<$ ppm-level).

On the one hand, the high signal rates, further away from the endpoint, are needed to obtain the required low statistical uncertainty. On the other hand, these high counting rates, of $> 10^8$ electrons per second, require the development of a new detector system, since the KATRIN focal plane detector system is limited to a total rate of 10^5 cps integrated over all 148 pixels. The second challenge is to control systematic uncertainties to the $<$ ppm-level in order to push the sensitivity to a parameter region competitive with indirect searches.

A key requirement on the new detector system results from the desired rate resolution. From a purely statistical point of view, a ppm sensitivity can be reached with a total statistics of 10^{16} electrons. Assuming a data taking period of 3 years, this leads to a count rate of $n_{\mathrm{tot}} = 10^8$ cps on the entire detector. To minimize the pile-up probability a count rate per pixel of maximally 10^5 cps is foreseen. This leads to a minimum of 1000 pixels. The maximum number of pixels is limited to keep the complexity and cost at a manageable level.

Beyond this rate consideration, the new detector system TRISTAN is optimized to minimize effects which can alter the shape of the detector response. The pixel-size is chosen to be 3 mm in order to minimize charge-sharing and pixel changes after backscattering and back-reflection [19]. The entrance window has a minimal thickness of about 50 nm, in order to minimize energy loss in the dead-layer, the detector size is chosen in a way to be placed in relatively low magnetic field, in order to avoid large incidence angles and decrease the loss of back scattered electrons. Detector and read-out electronics are optimized for low-noise and hence good energy resolution. Finally, a full waveform digitization with continuous reset, is chosen to minimize the effect of ADC nonlinearities. A detailed review can be found in [20, 21]. The details of the detector system are described in the following sections.

Besides a new detector system, studies show that the KATRIN experiment can be further optimized in order to comply the requirements of a keV-scale sterile neutrino search:

- The rear-end of the KATRIN beamline is realized by a gold-plated rear-wall. Backscattering of electrons off the rear-wall and Auger electron emission at the rear-wall can lead to a systematic effect of non-negligible size. In order to reduce the influence of the rear-wall related effects on the sterile neutrino search, we foresee to operate the the rear-end at low magnetic fields which magnetically prevents electrons from the rear-wall to enter the beamline. Moreover, low-Z material (such as Beryllium) is considered as an alternative material for the rear-wall [22, 23].

- To minimize scattering related uncertainties, the source will be operated at about 1% of the nominal density [22]. As the main measurement mode will be the differential mode, the stability of the activity is of minor concern.

- Along the tritium source tube (WGTS) electrons can be initially trapped in local magnetic field minima. They can leave the trap after a few scatterings, with reduced energy. This effect has to be precisely modelled, and if necessary compensation coils can be designed to mitigate the local magnetic field minima [22].

- In order to avoid non-adiabatic motion of the high-surplus electrons through the main spectrometer, the magnetic field in the main spectrometer needs to be increased. Simulations show that non-adiabatic transmission conditions can be eliminated at sufficient level, by an optimized magnetic field configuration [22].

A key aspect to minimize systematic uncertainties and to prevent the detection of a false-positive signal will be the combination of the different KATRIN measurement modes:

1. The integral mode is the nominal KATRIN mode for the neutrino mass determination. The detector measures the count rate of β-electron as a function of the retarding potential of the spectrometer. Thanks to the sharp electro-static filter, a ultra-high resolution of the spectrum at the eV-level is possible.

2. In the differential mode, the spectrometer is kept at fixed retarding potential and the detector is responsible for the energy determination of each β-electron. From a statistical point of view, the differential mode is preferred over the integral mode, since it allows for the highest signal electron collection (fixed, low retarding potential) and the lowest dead time caused by the ramping of the spectrometer.

3. Finally, it may be possible to apply the Time-of-Flight mode for the keV-sterile neutrino search, which would allow for a semi-differential measurement [24].

As the different measurement modes are prone to vastly different systematic effects, they would allow to cross-check a potential signal.

III. KEY DETECTOR TECHNOLOGIES

A. Silicon Drift Detectors

The TRISTAN detector has to cover a large area with a diameter of 20 cm. To handle the total count rate of $n_{\mathrm{tot}} = 10^8$ cps the detector must be segmented with several thousand pixels. The spectral analysis requires a good energy resolution of 300 eV FWHM at 20 keV, corresponding to an equivalent noise charge of 20 el. As backscattering of electrons will be a major source of uncertainty in the analysis, the insensitive thickness of the radiation entrance window has to be of the order of 50 nm or less. The sum of requirements decided in favour of a multi-channel Silicon Drift Detector (SDD) for the TRISTAN detector.

SDDs are a derivative of the basic principle of sidewards depletion: A volume of a high resistivity semiconductor, in our case n-type silicon, is covered by rectifying p-doped junctions on both surfaces. A small sized substrate contact in reverse bias to the p-regions depletes the Si bulk. In a SDD the p-junctions are strip-like segmented and biased in such a way that they generate an electric field with a strong component parallel to the surface. Signal electrons released within the depleted volume by the absorption of ionizing radiation drift towards the substrate contact, which acts as collecting anode. Due to the anode's small physical dimension, its capacitance has a small value almost independent of the detector area. Compared to a conventional diode of equal area, this feature translates to a larger amplitude and a shorter rise time of the output signal.

Originally, SDDs were designed and used as position sensitive detectors in particle physics in which the particle interaction point is reconstructed from the drift time of the signal electron. The semiconductor laboratory of the Max-Planck-Society (MPG-HLL) has developed an advanced design for X-ray and particle spectroscopy [20, 25]. Figure 3 shows the general concept of a SDD. The structures for the drift field generation and the collecting anode are placed on one side of the device, while a non-structured p-junction acting as a thin, homogeneous radiation entrance window covers the opposite surface 3. The simulated electron potential of a biased SDD is shown in figure 4. SDDs of this type combine are large sensitive area and a small value of the readout anode's capacitance. To take the full advantage of the small capacitance the first transistor of the amplifying electronics is integrated on the detector chip. The integration of the transistor minimizes the interconnection stray capacitance between sensor and amplifier. It guarantees an excellent spectroscopic resolution and operation at extremely high signal rates exceeding 105 counts per second. In addition, it makes the device largely insensitive to electronic pickup and microphony. The advanced process technology at MPG-HLL results in very small leakage current levels allowing for SDD operation at room temperature or with moderate cooling. As the SDD's bulk is fully depleted and irradiated through the non-structured thin backside entrance window, it has a high efficiency and a good low-energy response.

The SDD concept is very flexible in shape and size. However, the TRISTAN experiment would go beyond the inherent limitations of a single large detector in terms of drift time and count rate. Therefore, the TRISTAN detector will be based on multi-cell SDDs combining a large sensitive area with the energy resolution and the count rate capability of a single SDD. A multi-cell SDD is a continuous, gapless arrangement of a number of SDDs with individual readout, but with common voltage supply, entrance window, and guard ring structure.

Figure 5 shows the layout of the TRISTAN detectors' readout side with the field strip system and the readout transistor in each cell's center. The cells have a hexagonal shape for an optimum ratio of area and border length minimizing the fraction of split events. The size of a hexagonal SDD cell is 3 mm in diameter. The device has 166 cells and a total sensitive area of roughly $37 \times 37\,\mathrm{mm}^2$. The supply and signal lines of the individual SDD cells are connected to rows of wire bond pads placed along two edges of the chip. Based on this sensor format the concept of a four-side buttable module has been developed. The sensor chip is glued on the end plane of a cooling block. Components of the readout electronics as well as signal and power connections are placed perpendicular to the detector plane on the long sides of the cooling block. The focal plane of the TRISTAN detector will be built of 21 of these modules and cover an area of 21 cmin diameter. It will consist of almost 3.500 sensor and electronics channels. Figure 6 shows an exemplary TRISTAN SDDs array.

The response of SDD to electrons has been extensively characterized by means of multiple electron sources, in particular a scanning electron microscope (SEM) [25, 26].

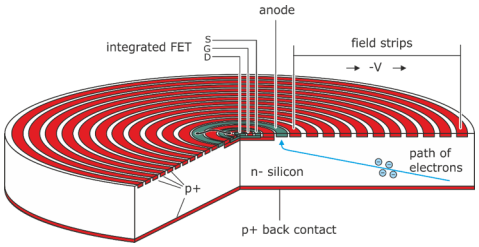

Figure 3: Schematic view of a cylindrical silicon drift detector. Signal electrons drift in the electric field towards the small sized collecting anode and the integrated amplifying transistor in the center of the device

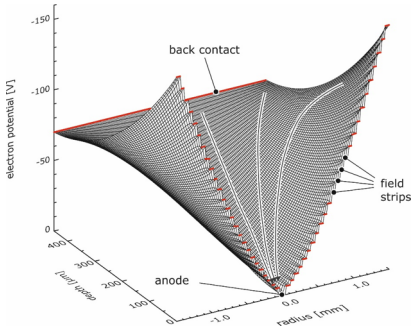

Figure 4: Simulated electron potential of a cylindrical silicon drift detector in operating conditions. The plot shows a cross section perpendicular to the surface through the center of the device. The arrows indicate the paths of electrons drifting to the anode.

B. Front-end ASIC

For the readout of the SDD array, a 12-channel front-end ASIC with an integrated nJFET (ETTORE) has been developed. The two-staged channel structure is depicted in Figure 7. The preamplifier is designed to work with the input JFET and the feedback capacitors both integrated on the detector chip.

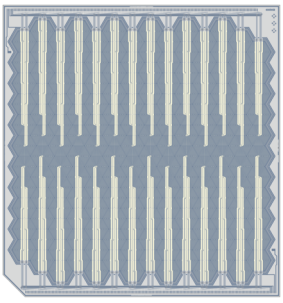

Figure 5: Layout plot of the TRISTAN SDD array with 166 hexagonal cells.

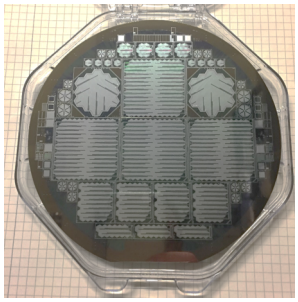

Figure 6: Photograph of a 6-inch wafer with four 166-cell TRISTAN detectors and small format test devices.

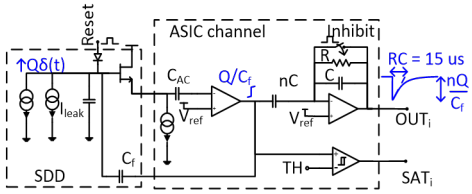

Figure 7: A schematic block diagram of a single readout channel of the 12-channel ASIC coupled to a SDD detector with an integrated JFET.

The first stage provides the biasing to the detector JFET and closes the preamplifier loop by connecting to the JFET source and to the feedback capacitance (Cf = 25 fF) for charge integration. After this stage, an AC-coupled amplifier provides an additional gain of factor n (selectable between the values of 5 and 10), and an exponential decay with a 15 µs time constant. The first stage output signal, featuring the classical ramp with superposed steps in correspondence of events, is meant to be read by a standard digital pulse processor or by an analog shaper. The second stage output signal requires a deconvolution operation (which might be performed both digitally or analogically) in order to be suitable for the standard processing.

The output impedance for both stages is 50 Ω. Assuming a capacitance of Cf = 25 fF, the maximum energy range (for photons) is 114 keV, The preamplifier is operated in a pulsed reset fashion with a dedicated diode which provides a periodical anode discharge and a signal that inhibits the ASIC during reset. Both components are integrated on the detector.

A comparator, whose digital output SAT_i is fed to the input of an OR-gate along with the outputs of the other 11 comparators, is used to detect the preamplifier output saturation. The resulting signal (SAT_{OUT}) is transmitted outside the ASIC to the external electronics, in charge of managing the detector reset. The ASIC also has a saturation input (SAT_{IN}), connected to one of the inputs of the aforementioned OR-gate; in multi-ASIC assemblies

(e.g. in the 166-pixel module), the SAT_{OUT} output of an ASIC can be connected to the SAT_{IN} of the neighbouring one, allowing to propagate the information about the saturation of any of the channels, so that only one physical line is needed for one full module. The full ASIC structure is depicted in figure 8.

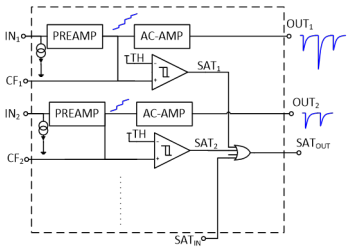

Figure 8: Schematic block diagram of the full ETTORE ASIC with the in- and output channels as described in the text.

C. Integrated TRISTAN module

The entire TRISTAN FPD (Focal Plane Detector) will be composed of 3486 SDD pixels subdivided in 21 identical modules; each module is based on a monolithic SDD matrix with 166 pixels. The module is an ensemble of electronics (front-end and detector) and mechanical structure (for cooling and support). A proper choice of the materials allows the operation in high B-fields and ultra-high vacuum as required by the project specifications.

Figure 9 illustrates the 166-pixel TRISTAN module indicating all its fundamental components which will be presented in the following paragraphs. Its development has been split in a series of intermediate versions with less pixels: based on 12- and 47-pixel monolithic SDD matrices.

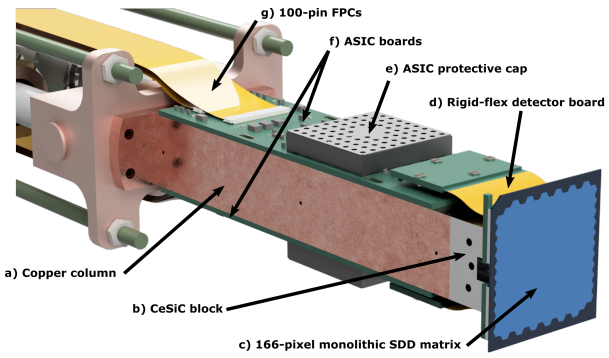

Figure 9: Overview of a 166-pixel TRISTAN module with the different sub-components. A detailed description of can be found in the text.

1. *Mechanical and cooling structure*

The detection module mechanical structure is based on two basic elements: the copper column (a) in figure 9) and the CeSiC block b). Both components have support and cooling purposes. The copper column, holding the two ASIC boards attached with four M1.6 screws each, is milled starting from a solid block. The choice of the material ensures good vacuum compatibility and great thermal conductivity ($385\,\mathrm{W/m\cdot K}$). The column is internally hollow to reduce its weight and is equipped with holes to evacuate the internal volume from air.

The coupling between the silicon detector and the support structure is a critical point due to the difference in terms of coefficient for thermal expansion (CTE) between the copper ($17\cdot10^{-6}\,\mathrm{K^{-1}}$) and the SDD ($2.56\cdot10^{-6}\,\mathrm{K^{-1}}$ considering pure Si). Due to the CTE mismatch and the large area of the SDD matrix, the detector would be damaged by the wide temperature range which will experience, from bake-out temperatures of approximately $100\,^{\circ}\mathrm{C}$ to the operating temperature of $-40\,^{\circ}\mathrm{C}$. For this reason, the SDD matrix is glued with epoxy to a machined CeSiC part which is in turn mounted on the copper column. CeSiC is a special ceramic material based on silicon carbide which is characterized by high specific stiffness, high strength, and good machinability. It offers also excellent thermal conductivity ($121\,\mathrm{W/m\cdot K}$) and a low CTE of $2.09\cdot10^{-6}\,\mathrm{K^{-1}}$ at 300 K which is well matching the CTE of the silicon detector.

2. *On-module electronics*

The two ASIC boards (marked as f) in figure 14) are the core of the on-module electronics. Both are identical and each one provides power supply and signal preamplification for 83 pixels. Each ASIC board hosts 7 ETTORE ASICs which are glued to the PCB with epoxy and are wedge bonded using Al-Si wire. The boards are protected by an amagnetic cap with venting holes e) directly soldered on the PCB. The power supply for the ASICs is provided by an on-board ADM7154 ultra-low noise high PSSR 3.3 V LDO regulator. The ASIC board implements passive filters without inductive components for all SDD and ETTORE power supplies, static bits, and voltage references. The SDD reset diode line presents a small capacitive coupling to the anode of each pixel and is a possible injection point for external noise. Due to the nature of the signal present on this line a passive filter cannot be employed and a special actively gated filter is implemented on the ASIC board. Before the gluing and bonding of the ETTORE ASICs the PCB is assembled with all the required components using solder paste with no-clean flux and undergoes an ultrasonic cleaning and vacuum drying procedure.

Power supplies, output signals and other control lines for each 166-pixel detection module are carried by 4 custom polyimide-based flexible printed circuits (FPCs)

100-pin each g). These FPCs offer a very compact and dense interconnection from the ASIC boards, where the space constraints are particularly tight, to the vacuum feedthrough. Each FPC is characterized by the presence of two copper layers, signals and grounds are interleaved both inside the same layer and between the two layers to reduce capacitive coupling between lines and enhance the signal integrity. The FPCs mate on both ends with Hirose FH29DJ-100S-0.2SHW SMD connectors.

Each SDD matrix hemisphere is connected to the ASIC board by means of a rigid-flex board d). This PCB employs a special rigid-flex process characterized by a 3-layer 200 µm-thick flex section and two 5-layer rigid ends having two different total thicknesses (1.6 mm on the ASIC board side and 0.6 mm on the SDD bonding side). On the SDD side, the detector is wire bonded to the PCB, on the ASIC board side, the connection is made by means of a Samtec ZA1-20-2-1.00-Z-10 dual compression interposer array with 200 pins. The SDD signals are divided in two classes: FB (feedback lines) and SC (source lines). The two signal classes travel in the rigid-flex PCB in separate layers with an additional ground layer in the middle with shielding purposes.

The 166-pixel module has a single ground for signal and power, and is shared between the two ASIC boards by means of the copper column. Despite having a single on-module ground, in the interconnection to air-side electronics a distinction between the signal ground and the power ground arises. The former ground lines carry only the return currents of the single ended output signals (pseudo-differential readout might be implemented with ground sensing), while the latter ground lines carry the power supply return currents.

The SDD matrix is operated in a pulsed reset regime, with independent reset signals and saturation outputs for each hemisphere. However, due to the currents generated during the reset phase it is very likely that the two hemispheres will be operated by a single synchronous reset.

3. *Vacuum compatibility*

The detector chamber is directly connected to the main spectrometer, which is operated in an ultra-high-vacuum (UHV) of up to 10^{-11} mbar. Its vacuum system [27] includes getter pumps with an effective pumping speed of 250 000 ℓ/s (hydrogen) as well as six turbo-molecular pumps (TMP) with an approximate pumping speed of 5000 ℓ/s for non-getterable gases (e.g. hydro-carbons). In the main spectrometer section, the outgassing of the stainless steel walls is the main source of gas that limits the final pressure. In the much smaller detector section, the main source of pressure increase is caused by the outgassing of electronic components (hydro-carbons). In order to achieve the UHV in the main spectrometer, the maximum allowed gas flux from the detector section has to be smaller than 5×10^{-8} mbar ℓ/s. It should be noted, that the background and hence vacuum requirements for

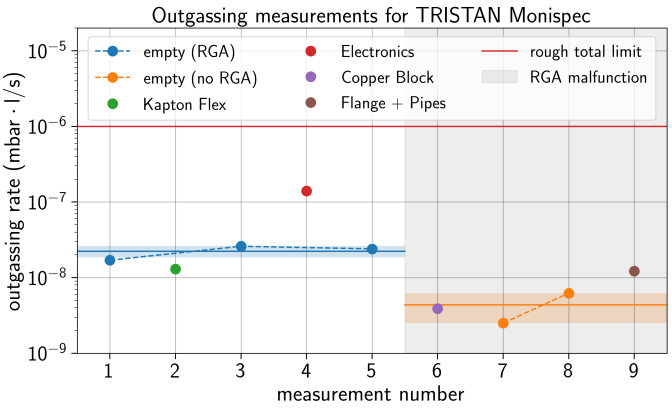

Figure 10: Measured total outgassing rates of the components for the integration of the first TRISTAN module at the monitor spectrometer. In between probe measurements, the outgassing of the empty vacuum chamber is measured to determine the background. The lower horizontal lines and shaded areas correspond to mean and standard deviation of the measured background values.

a sterile neutrino search with KATRIN may be less stringent than for a neutrino mass measurement.

The materials of the detector modules, cables, and internal mechanical structures have to carefully selected with regard to their outgassing rates. In addition, all materials should be able to be heated up to temperatures of up to 100° C in order to reduce the outgassing by out-baking. Figure 10 shows the results of outgassing measurements. All components have been baked-out at 100° C and kept under vacuum conditions for two days before the outgassing measurement. The highest outgassing rate is observed for the printed circuit boards (PCB) of the pre-amplifier boards, which have to be placed close to the detector inside the vacuum chamber. Since the total outgassing rate of the 21 detector modules would be above the maximum allowed gas load, the design of the detector chamber includes a tight-fitting mechanical shield, covering the gaps between the detector wafers and the wall, thus reducing the conductance between the rear part of the detector modules with the PCBs and the front side of the SDDs facing the spectrometer. UHV pumps installed at the rear section of the detector chamber have to provide a two orders of magnitude larger effective pumping speed than the conductance to the front section. This vacuum system will consist of a combination of cascaded TMPs and getter pumps.

The detector modules will be cooled down to an operating temperature of about −40°C. On the one hand this low temperature will reduce the outgassing rate of the materials, on the other hand hydro-carbons with lower vapour pressures can condensate on the cold surfaces. In particular the front face of the SDD-wafer could accumu-

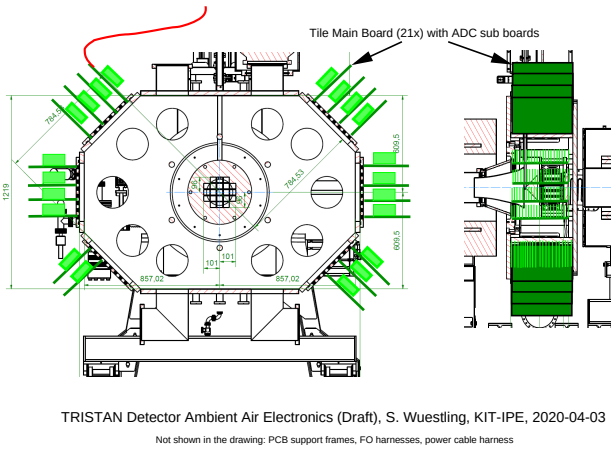

Figure 11: A schematic view of the ambient air electronics of the TRISTAN detector system. The 21 TMPs are displayed in green.

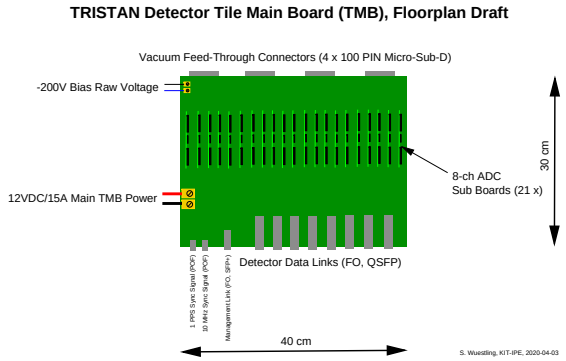

Figure 12: A sketch of the TRISTAN Detector Tile Main Board (TMB). It integrates the 8-channel ADC sub-boards as well as the different power supplies and signal output.

late a layer of hydro-carbons which would slowly increase the dead-layer of the detector over time, affecting the energy resolution. These effects can be mitigated by the additional vacuum shield that separates rear and front of the modules.

D. Ambient air data acquisition system (DAQ)

The TRISTAN detector ambient air electronics are located outside the TRISTAN detector chamber. The detector chamber has a prismatic shape with an octagonal cross section in the current stage of design and is shown in figure 11. Six of the eight outer surfaces of the octagon are intended to carry electric vacuum feedthroughs, preferably as 100pin Micro-Sub-D connectors.

During operation, the detector chamber is on post-acceleration high voltage potential of up to +25 kV. The ambient air electronics must therefore be powered via an insulation transformer, and all data up- and downlinks have to be realized as fiberoptic links. The basic DAQ system structure proposed here is based on early digitization with ADCs that are - in contrast to most commercial DAQ systems - detached from the following digital data processing sections, which perform pulse processing, histogramming, computer access for mass storage etc. The advantages of this structure are:

- smaller number of project-specific building blocks (digital main DAQ-section will consist of standardized FPGA boards in a standardized rack system),
- rugged commercial high-speed digital fiberoptic data links,
- easy high-voltage insulation of front-end electronics,
- short analog signal paths,
- flexible, reconfigurable data processing in the digital domain.

The basic idea of the concept presented here is to partition the ambient air electronics into 21 tile main boards (TMB) with one TMB serving one detector tile with 166 SDD detector channels each. The conceptual design can be seen in figure 11 and fig 12. Digitization is performed on 21 ADC sub-boards with 8 channels each that are integrated on the single TMBs. Two digitizer channels of the 21×8 total channels on a TMB will be unused. The pin count required to connect one TMB to the in-vacuum electronics is estimated to be 400, provided by four 100-pin Micro-Sub-D vacuum feed-throughs in a row, that fit into the 40 cm detector chamber. 166 differential channel signals require 332 pins, 68 pins are left for the power&control signals for the in-vacuum electronics. If required, more feed-throughs can be placed in between the rows carrying the TMBs and be connected to the latter via ribbon cables.

The here described general design parameters can be used to estimate the total down-link payload data rate per tile (assuming a 16-bit ADC resolution and 100 MSps sampling rate):

$$166\,\text{pixel/tile} \times 16\,\text{bit} \times 100\,\text{MSps} = 265.6\,\text{GB/s tile}$$

Another design criterion takes into account that the detector chamber is located between two superconducting magnets. The stray field which the detector ambient air electronics will be exposed to is in the order of 100 mT, which excludes any ferromagnetic components.

1. Options for the main DAQ

The main DAQ is the part of the DAQ system located outside the magnetic field of the detector apparatus and on normal earth ground potential. The function of the main DAQ is digital pulse processing consisting of, for example, trapezoidal filtering, threshold discrimination, energy and timing determination, histogramming, charge-sharing identification, and others. As a hardware platform for this part of the DAQ, it is aimed for the usage of non-custom FPGA cards residing in a standardized rack. Options currently envisioned are:

- QSFP optical links and *Helmholtz* AMCs (Advanced Mezzanine Cards) residing in MTCA.4 racks, 2 detector tiles per rack, 11 racks required (least density option)
- QSFP28 or Firefly optical links and up to 4 CMS *Serenity* cards residing in 1 ATCA rack (highest density option). These high-performance FPGA cards have been designed at KIT-IPE for the CMS detector at the LHC.

2. Functions of the tile main board

The primary function of the tile main boards (TMB) is the digitization and transmission of the detector signal. The in-vacuum ETTORE front-end drive the detector signal through the in-vacuum cables and into the TMB. On the TMB the signal is either directly fed to the ADC sub board or, if required by the limited drive capability of the ETTORE chips, buffered before. Further tasks of the TMBs are:

- Provide a clean sampling clock and timing for the ADC sub boards. The timing is based on two sync signals: one with a 1 PPS (pulse per second) and another with 10 MHz. Both signals are received via fiberoptics from a central timing controller that can reside remotely. The jitter cleaning corrects the phase noise picked up on transmission from the central timing control.
- Serialize ADC data, regroup and format it for fiberoptics transmission and send it to the fiberoptics transceivers.
- Handling management data via: ADC configuration, PGA configuration, configuration of the ETTORE RESET concept, controlling the bias DACs, controlling test pulse DACs, performing auxiliary functions (temperature, current, voltage measurements and other slow readbacks).
- Supply, diagnosis and control of the in-vacuum electronics.

3. TMB power supply concept

The power dissipation of a TRISTAN TMB (with 21 ADC sub boards) is estimated to be in the range of 100 to 150 W. On the TMB, a variety of different supply voltages will be required. The basic idea of the proposed power supply concept is to provide magnetic-field compatible (air-coil) DC/DC converters on the TMB to derive all these voltages from a sole primary power supply voltage. As the EMC behaviour of step-down converters worsens with an increasing step-down ratio, a balance must be found between a low step-down ratio and the occurrence of excessive supply currents on the cable harness, feeding the 21 TMBs from a remote isolated power supply. An optimum was found for a power supply voltage of 12 V, partitioned in up to 5 groups of TMBs. Assuming a supply current of 15 A leads to a total current of 315 A for all TMBs combined.
Independent of the common power supply voltage, the raw bias voltage of -200 V is fed in separately. As the current demand for SDD biasing is low, all the respective (negative) voltages can be derived with linear regulators from this voltage. This eases the task to provide clean bias voltages to the SDD and avoids the requirement for step-up DC/DC converters on the TMB.

4. The ADC sub boards

In order to achieve a reasonable scale of integration, 8-channel ADCs will be used. Apart from the 8-channel ADCs, the ADC sub boards will comprise an ADC driver operational amplifier for each channel. This amplifier is incorporated into an anti-aliasing (AA) filter circuit respectively.
For the TRISTAN detector system it is planned to perform a redesign of an already existing 8-channel ADC card that has been designed and built at KIT-IPE. The card has the following properties:

- It includes an AA-Filter of 5th order Bessel, 2nd order active Sallen-Key plus 3rd order passive LCR with a ceramic core Ls. The Bessel-type low-pass filters are particularly well suited for pulse processing due to their close to constant group delay over frequency.
- The ADC *AD9257* (analog device with 14-bit) has a sampling rate up to 65 MSps.
- The programmable gain amplifier *PGA5807A* (Texas Instruments) offers full-scale ranges from 63 mVpp to 500 mVpp.
- It allows for a fully-differential signal handling.

5. Timing and clocking concept

The clocking concept proposed for the TRISTAN detector system is hierarchical. The master timing unit is a GPS clock with multiple fiberoptic outputs. It provides an absolute timebase that can be read out by the digital pulse processing implemented into the main DAQ system. Synchronization among the DAQ system and the TMBs is provided by 1 pulse per second and 10 MHz signals distributed by balanced fiberoptic lines in a star topology from the GPS clock.
On the individual TMBs, all required clock signals are derived from the 10 MHz master clock provided by the GPS clock. ADC sampling clocks are jitter cleaned and distributed among the ADC sub boards. DC/DC converter clocks are phase-locked with the ADC sampling clock. This avoids beat frequencies forming between independent clocks or their harmonics. As a consequence, all ADCs in the detector system and all DC/DC converters operate synchronously.

6. DAQ development phases

In correspondence to the integration of the whole detector system (see section IV), the plan for the DAQ development is divided into several phases:

- *Demonstrator phase*: During the first integration stage of the detector system (phase-0), a TRISTAN TMB is not yet available. However, at KIT-IPE, the concept of the detached ADCs will already be evaluated using the application at the existing KATRIN Focal Plane Detector (FPD). Currently, the ambient-air FPD electronics consists of so-called optical sender boards which contain analog fibre-optic drivers that transmit the detector channel data through plastic optical fibres. The system consists of four optical sender boards serving 37 channels each. For the concept with the detached ADCs, each optical sender board is replaced by a 40-channel digitizer main board, called RADC-40 board. It transmits raw digital ADC output data through a QSFP digital fibre-optic link. The 8-channel ADCs are located on individual mezzanine ADC boards, that also contain an 8-channel programmable-gain amplifier and anti-alias filters.In the TRISTAN phase-0 scenario, one such digitizer main board will serve 36 out of the 166 channels of the only detector tile existing in this phase. Depending on the number of available RADC-40 boards, up to five of them can be fitted in a suitable sub-rack, enabling the readout of all pixels of the 166-pixel detector tile. Digital waveform processing occurs in *Helmholtz AMC* FPGA cards residing in an MTCA 4 system, that also comprises a Linux-based DAQ computer.
- *9-tile phase*: In the second stage, the DAQ system is planned to have the final structure, consisting of the final tile main boards (TMB) and the final digital DAQ section.
- *21-tile phase*: The previously used DAQ will be scaled up to 21 tiles by adding more tile main boards and *Serenity* FPGA boards, and a stronger power supply.

E. Calibration of the detector system

In the KATRIN experiment two calibration systems are installed for calibrating the focal-plane detector (FPD): one with a gamma-ray source, to determine the absolute energy scale precisely, and a second one exposing the detector to keV electrons, to probe the response to electrons which is much more affected by the detector's surface properties than in the case of gamma rays. Both these systems can be scaled to suitable performance for the TRISTAN detector system.

Beyond that, for TRISTAN, electron sources, which allow to calibrate and characterize the full beamline response, need to be applied. These entail the rear-section e-gun and a gaseous krypton source, which can be co-circulated with the tritium gas.

1. Calibration with gamma radiation

A ^{241}Am source is used to expose the detector to gamma rays. It features multiple gamma and X-rays in an energy range of $10-100$ keV, most importantly for calibration the two strongest gamma lines at 59.5 keV and 26.3 keV with comparably high branching ratios above one percent. With a half-life of 432 y the source will not have to be replaced during the lifetime of the experiment. The source is inserted by putting it in a tube that is connected with a bellows to the beam tube and can be inserted into the beam line about 1 m in front of the FPD. The insertion system with inserted tube is shown in the open beamline in figure 13. During regular measurements the tube is retracted and the source is extracted and stored far from the detector.

The rate at which the calibrations have to be performed depends on the gain stability of the full signal chain, which is for example affected by temperature drifts of electronics. The necessary exposure time for a single calibration depends on the required precision for the peak position. With several 1000 counts in the important peaks, the relative uncertainty in the position should be around the 1% level of the resolution, adding negligibly to the overall resolution.

For TRISTAN the following parameters will change with respect to the existing structure: the distance of the sources to the detector will increase with the current design from 1 m to about 1.6 m and the pixel size will decrease from 44 mm^2 for the FPD to about 6 mm^2. The

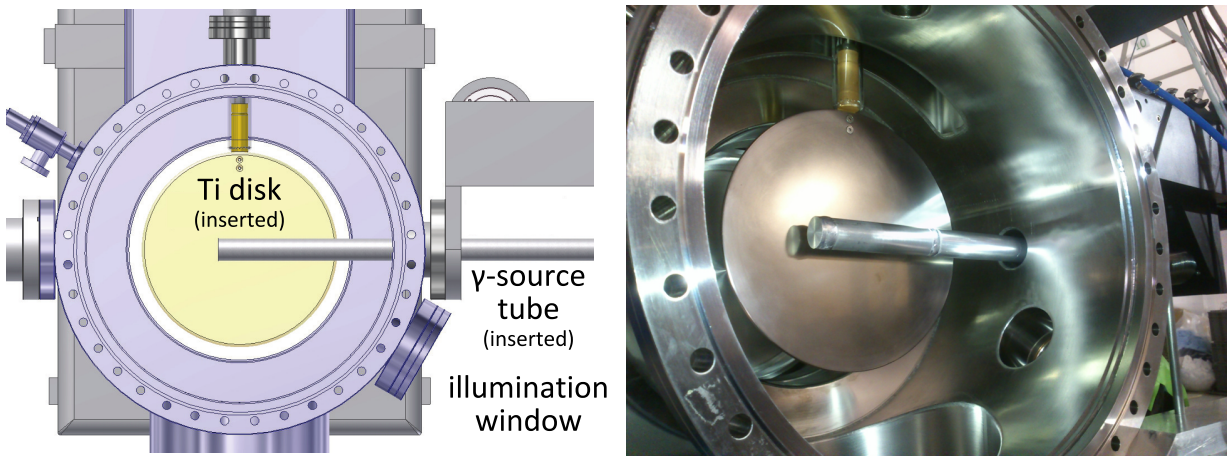

Figure 13: The two calibration systems for the FPD in KATRIN. For calibration with gamma rays a ^{241}Am source is inserted into the thin tube in the front which is shown fully inserted into the beam line and can be retracted during regular measurement. The titanium disc behind the tube can be illuminated with UV light through a sapphire window in the lower right of this beam tube segment to create photo electrons which can be accelerated towards the detector for probing its response to β-radiation.

rate depends roughly quadratically on the distance d, and linearly on the pixel size A, thus, it will approximately decrease by a factor of $\frac{R}{R_0} = \frac{d_0^2 A}{d^2 A_0} \approx \frac{1}{20}$. This decrease can be compensated by acquiring a stronger source. The current source was manufactured by Eckert and Ziegler and has a nominal activity of 18.5 MBq. Similar sources are available with activities of up to 18.5 GBq.

2. *Calibration with β-radiation*

For calibrating the FPD of KATRIN with β-radiation a titanium disk, stored in a compartment above the beam line, is lowered with a pneumatic motor into the beam line. The disk is located about 1 m in front of the FPD, directly behind the insertion point of the gamma source (see figure 13). Photo electrons can be generated by illuminating the disk with UV diodes at a wavelength of 250 nm through a sapphire window close to the disk (lower right in figure 13). A voltage of 0-25 kV can be applied to the disc, which in addition to the 10 kV of the post post acceleration electrode, generates a mono-energetic electron beam with an energy of 10-35 keV.

For TRISTAN the higher distance of the detector to the disk does not matter, as the electrons are magnetically guided and their intensity does not decline with distance. The approximately 10 times smaller pixel surface can be compensated by applying a increased voltage to the UV diodes. Furthermore, the existing UV diodes can be replaced by other, more intense light sources which are commercially available.

3. *Full system calibration*

For TRISTAN is will be of key importance to precisely calibrate and characterize the entire beamline. As in the usual KATRIN mode, individual parameters (such as B-fields, column density, etc.) will be determined with dedicated calibration and monitoring devises. Additionally, we aim for a measurement of the differential energy spectrum of mono-energetic electrons passing the entire beamline.

An ideal calibration source are the mono-energetic electron lines of the gaseous and solid ^{83m}Kr sources. The gaseous krypton can be co-circulated with the tritium gas, allowing to characterize the impact of scattering and trapping in the source, as well as energy broadenings due to electric potential variations in the WGTS. The solid krypton source at the location of the cryogenic pumping section (CPS), may be of interest to disentangle various effects.

The angular- and energy-selective electron gun at the rear end of the experiment allows to calibrate individual pixels as a function of energy and angle, including energy losses due to scatterings in the WGTS. Moreover, dedicated Time-Of-Flight (TOF) measurements to determine the energy loss function for lower electron energies will provide a key input to the spectral analysis in a wide energy range.

An interesting approach to calibrate the full beamline, may be with the help of the ultra-high energy resolution of the main spectrometer. The tritium spectrum itself would be truncated sharply and two close-by retarding potentials. The difference of the two resulting differential spectra measured at the TRISTAN detector, represents the response of the system to a narrow energy spectrum, where the width of the initial spectrum is given by the

distance of the two retarding potentials.

A combination of all calibration systems will allow to disentangle the individual experimental effects arising from the source, spectrometer and detector section.

IV. PHASES OF SYSTEM INTEGRATION

We propose a step-wise project progress with three different phases (0-2). The phases show an increasing level of technical complexity with regard of the integration of TRISTAN detector modules into the KATRIN beamline. As a single TRISTAN detector module the mechanical unit is defined, which carries the SDD detector and the first stage electronics (see figure 14). The phase-wise approach is in order to minimize technical risks while maximizing scientific output and keeping shut-down times for data taking as short as reasonable. The details of the phases are described in the subsections, however, the basic considerations are:

Phase-0: Integration of one module at the Monitor-Spectrometer (MoS) with the purpose to demonstrate the high spectroscopic performance of a TRISTAN module for electrons in a high magnetic field and meeting a ultra-high vacuum standard. This phase stared in November 2020, first results are described in the following section. Once commissioned, the physics output is defined by the HV monitoring of the MoS or at a later point of time by examining solid state sources (e.g. weakly loaded tritium films).

Phase-1: Integration of 9 TRISTAN modules in the KATRIN beam line by replacing the current KATRIN detector (FPD) and its existing detector platform infrastructure. It allows measurements in the standard neutrino mass mode giving additional access to detector systematic effects with significant better signal to background ratio, higher position resolution and higher allowed data rates. Despite expected limitations in post-acceleration performance (+10 kV instead of planned +30 kV) a competitive sensitivity for the keV-sterile neutrino search is already given in such a setup (see blue solid line in figure 2). The TRISTAN phase-1 system, including optimized electronics and DAQ system, can be ready for installation by the end of 2024, requiring less than half a year for commissioning. The short integration time is due the adaption of the phase-1 design to the existing FPD environment and testing in a FPD environment replica. All electronic and DAQ parts are designed for scalability to 21 modules.

Phase-2: The last stage of integration contains the upgrade to 21 TRISTAN modules behind the detector magnet in an optimized electro-magnetic setting. By using an additional super conducting magnet the magnetic field at the detector entrance can be chosen as low as 0.8 T, which optimizes the trade-off between backscattering and detector size [19].

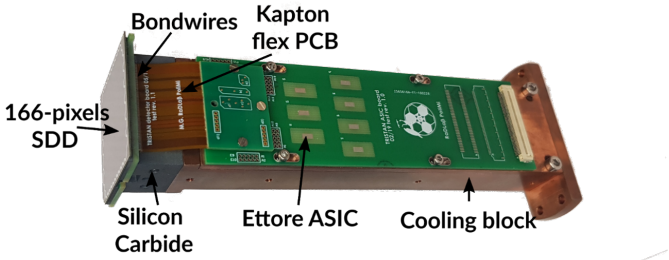

Figure 14: Photograph of a TRISTAN detector module. It comprises the multi-pixel SDD and the 1^{st} stage electronics. They are mounted on a copper block, which serves as interface for the system integration into the KATRIN beamline.

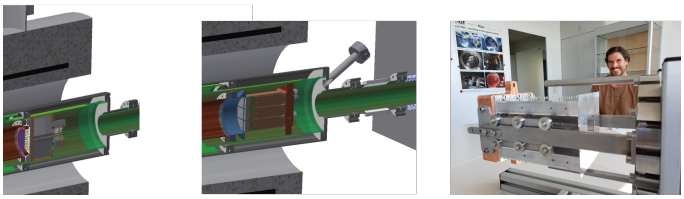

Figure 15: Left: Half-cut of as-built design of FPD inside warm bore of detector magnet; middle: replacement of FPD detector flange with phase-1 tower (9 modules); right: photo of 1:1 mock-up of phase-1 tower

A. First results of phase-0

In the phase-0 of the TRISTAN project one detector module is integrated into the monitor spectrometer of the KATRIN experiment to test the feasibility of the detector system design in interaction with a KATRIN-like environment. It serves as an excellent test bench for the concepts that went into the TRISTAN design to validate it and if necessary modify it.

A module is mounted on an 80 cm long cooling and holding structure to place the detector near the magnet. At the tip of the structure the heat exchange block is installed. It is connected to two cooling pipes that carry the thermal liquid to cool the detector below -40° C. To release stress from the cooling pipes additional support rods are placed on the upper and lower half of the structure. An electrical insulation between the in-vacuum

parts and the rest of the system is provided by ceramic insulators at the air side of the cooling pipes and the stiffeners in vacuum. To ensure the compatibility with vacuum and magnetic fields (up to 0.5 T at the position of the detector) the entire structure is made out of non-magnetic stainless steel. Additionally to further reduce the impact of outgassing parts (mainly the electronic boards) on the main vessel vacuum, a vacuum shield is placed in front of the detector. Its task is to reduce the conductance between the detector chamber and the main vessel. The vacuum shield is fixed as close as possible to the outer edge of the SDD-chip, with a remaining gap of approximately 0.5 mm. The outer ring is made out of stainless steel and PEEK and is inserted at the downstream side of the vacuum cross. When installing the detector system, the vacuum shield and the outer ring align with each other, closing the remaining gaps to the vacuum walls. Additionally, the outer ring centers the detector system and electrically and thermally insulates the structure from the vacuum chamber. To further improve the vacuum in the system, one turbo molecular pump and one getter pump are placed directly in the detector chamber. With the help of these measures, a vacuum level of 10^{-9} mbar was reached in the spectrometer vessel.

As described in section III C the detector module consists of a 166 pixel SDD which is connected to two ASIC boards via the C-Shape flex cables. Each ASIC board is coupled to two 100-lines Kapton flat cables, which route the signals and power lines over a distance of 80 cm towards the flange. At the flange level each Kapton cable is adapted to a 100 pin Micro-Sub-D connector via a small PCB board. On the other side of the flange in air all lines are connected to the Bias Board. It consists of a control board that manages the required voltages for the module and multiple signal buffer boards that amplify and buffer the signals for further transport to the DAQ. For the setup in the monitor spectrometer in phase-0 the so-called KERBEROS DAQ is been used (see figure 16).

KERBEROS is a 48-channel Analog Processing Platform and DAQ system for the readout of large SDD arrays. It has been developed for the testing and characterization of the detector modules of the TRISTAN experiment [28]. The platform main components are: the analog processing ASICs (SFERA), the high linearity SAR ADCs (Linear Technology LTC2386-16) and a Xilinx Artix-7 FPGA Module (Enclustra AX3).

The detector analog signals can be connected either via individual SMA coaxial connectors or via compact 2 mm header connectors carrying 12 channels each. KERBEROS inputs are routed to the analog chip, SFERA, where they are processed and filtered by a semi-Gaussian Shaper. Then, the peak amplitude of the output pulse is sampled and buffered before being digitized by the off-chip ADC. This function is performed by SFERA Peak Stretcher circuitry, which is responsible for the peak detection and the exclusion of partly overlapped pulses, together with the pile-up rejector logic. Consequently, the data is multiplexed and sent to the external analog

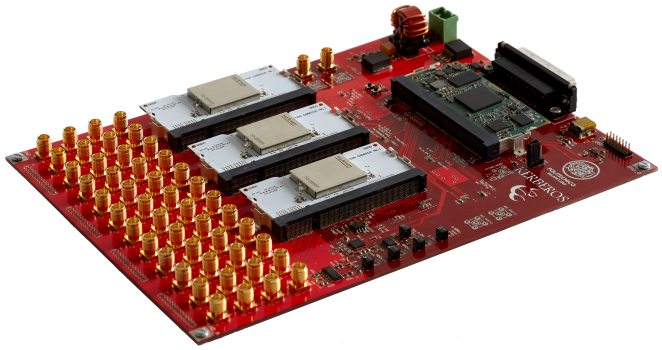

Figure 16: Kerberos Platform ($160 \times 220\,\mathrm{mm}^2$). The analog input connectors are placed in the left part of the board. In the center it accommodates three SO-DIMM sockets for the SFERA ASIC carrier PCB (white). The right side shows the FPGA module (green) and the output connectors.

to digital converter (ADC), an LTC2386-16 from Linear Technology. The ASIC and the ADC design has been replicated three times, in order to reach 48 analog input channels.
The communication between the different components as well as the implementation of the different readout multiplexing strategies and the data transmission with host PC is performed by the Artix-7 FPGA.

For the TRISTAN SDD characterization, it was chosen to use the burst readout, where all the channels are simultaneously sampled as soon as one valid event is recognized. This will trigger all three SFERA ASICs at the same time, providing a complete map of the detector at that time while at the same time allowing to measure back-scattering and charge sharing coincidence times. A complete scheme of the platform can be seen in figure 17, where the main blocks are highlighted.

For the first acquisition, a 47-pixel TRISTAN module at the monitor spectrometer in combination with the KERBEROS DAQ was used. Figure 18 shows the spectra of mono-energetic conversion electrons from ^{83m}Kr decay. The measured width of the L_3-32 peak is homogeneous over the detector pixels and reaches 325 eV to 362 eV FWHM at 30.5 keV, as shown in figure 19.

B. Status and planning of phase-1

Phase 1 stands for the integration of 9 modules as a quasi replacement of the current Focal Plane Detector inside the warm bore of the detector magnet. These 9 modules are arranged in a 3x3 matrix and build together the so-called phase-1 tower (see fig. 20). The sensitive area amounts to 10400 mm^2 for a circular, centered flux tube with a diameter of 127 mm diameter (i.e. filling

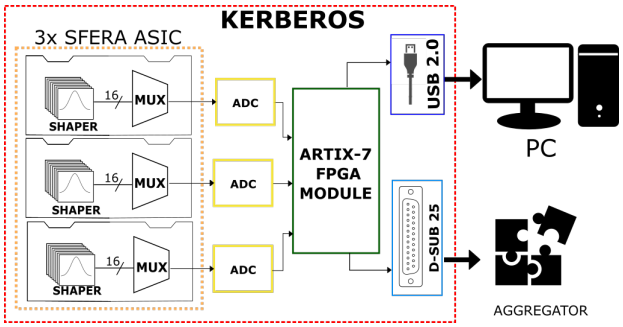

Figure 17: Schematic diagram of KERBEROS platform main components. The analog pulse processor SFERA (orange) output is digitized by the on-board ADCs (yellow). The FPGA (green) is tasked with the signal regulation and external communication either via USB (purple) or a D-SUB 25 connector (blue).

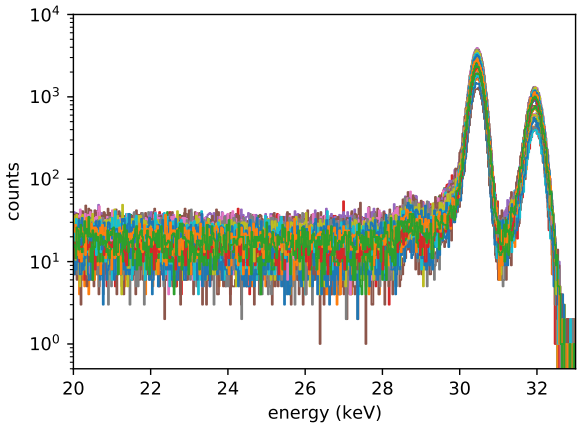

Figure 18: Acquired spectra with a TRISTAN module in the monitor spectrometer setup. The two peaks correspond to L_3-32 and MN-32 conversion electron lines from ^{83m}Kr. The detector has 47 pixels, of which 43 could be read out and are superimposed in this plot.

factor of 80%). Such an instrument will already allow for world-wide competitive searches for the sterile keV neutrino. In figure 2, we show the sensitivity of a Phase-1 measurement, with 0.3% tritium activity, a retarding potential of 8 keV, and a total measurement time of 6 month. Also as mentioned such a detector system allows for complementary systematic measurements for the neutrino mass analysis. A TRISTAN detector could measure more precisely systematic effects, in which the analysis benefits from the much higher energy resolution, higher spatial resolution and lower pile-up effects.

The design of phase 1 is deliberately driven by minimizing the environmental changes of the current detector infrastructure, especially making full use of the existing pinch and detector magnets and the long gained experience of the beampipe environment behind the spectrometer. The integration is thought as an exchange of the FPD detector wafer flange with an interface flange, which carries the 9 TRISTAN modules (phase-1 tower). The similarity of the new design to the existing one is shown in the left and middle pictures of figure 15. We assume that the mechanical implementation of the new system is achievable during a slightly extended KATRIN maintenance period of 4 months.

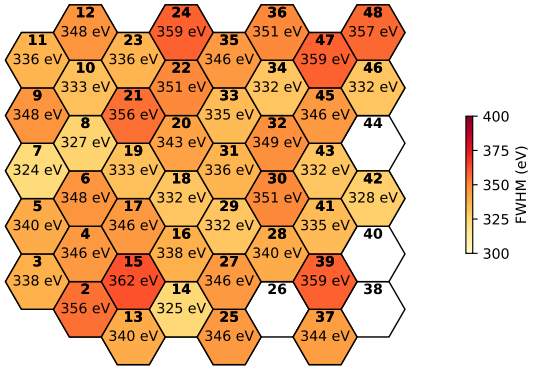

Figure 19: Pixel-map of the 47-pixel TRISTAN module. The measured FWHM of the 30.5 keV peak from conversion electrons is shown for 43 of the 47 pixels.

Figure 20: A matrix of 3x3 modules builds the phase-1 tower (inner module missing here).

The key features of the conceptual design of the TRISTAN module integration to match the design drivers are described in the following paragraphs:

The nine TRISTAN modules are packed as close as possible into a 3x3 array with a target of a 0.3 mm gap in between them. They are mechanically fixed to an interface flange. This interface flange is attached to the end

flange of the post acceleration electrode and provides the mechanical fixing point. The interface flange carries also a metal grid, which is aligned to cover the gaps between the modules. The diameter of the sensitive area of the detector surface amounts to 127 mm. A slight shift of the detector surface by a few mm in z-direction is expected in comparison to the FPD but this will not play a significant role in the imaging properties of the flux tube. In the design process we decided to foresee the option of additional cooling of the copper modules. The additional cooling will be provided by a oil fluid circuit through a cooling block. The cooling block will be connected by flexible braids to the TRISTAN modules.

Maintaining the vacuum integrity of the system towards the main spectrometer is one of the technical challenges. As mentioned, in the current FPD setup the detector flange completely separates the space containing the electronics in a leak tight fashion from the main spectrometer volume. Therefore, in the current design of the FPD all sealings of this electronic space are non-metal sealings and not compatible to XUHV requirements. The modification of these sealings of the detector environment to XUHV standard means the mechanical modification of the beam tube. Therefore flanges have to be cut, modified and again welded. Due to the long experience of the KATRIN experiment with such issues we regard this as technically feasible. The stronger challenge arises from the outgassing of the electronics towards the main spectrometer. The technical design will address here a higher pumping speed in the detector section and minimizing the conductance towards the main spectrometer.

The mechanical setup and dimensions will remain nearly the same in phase 1 as compared to the current KATRIN situation. However, due to the additional cooling lines to stabilize cooling, the veto and lead end cap will have new openings at the rear side of the detector chamber. The expected background increase due to external radiation onto the detector is assumed to be negligible for the search of sterile neutrinos or analysis of the entire tritium spectrum.

In order to achieve the original PA requirement of +30 kV biasing in a high magnetic field (3T) the PA design could be revisited and the PA electrode newly built. However, this would mean substantial modifications to the detector environment as it would call for a complete redesign of the post acceleration electrode and the EMD setting. This would be in conflict to the phase-1 strategy to minimize environmental changes of the detector section in order to achieve a smooth and efficient phase-1 operation. Keeping the PAE situation as it is, is one of - if not the major - key aspect of the phase-1 design.

Definitively it needs a significant increase of signal feedthroughs. In the optimal case each pixel is read out in differential mode. Thus at least $9 \times 166 \times 2 = 2998$ signal feedthrough pins are required. In our conceptual design this will be realized with the Sub-Micro-D standard. The project is in advanced studies with a commercial supplier for a 3600-pin solution (36 feedthroughs).

C. Quality assurance and progress monitoring

The system integration of each phase is supposed to happen within the framework of the KATRIN project. Therefore, we apply the standard procedures for quality assurance and progress monitoring, as established at KATRIN during its assembly period and routine operation. In particular:

- Initial "Operation Mode Announcement" to the start of the project.
- Progress reports (oral or written) at regular steering meetings (e.g. Executive Board, Collaboration Board, KIT Steering Committee, Collaboration Meeting).
- Topical reports on request to the KIT project management or Executive Board.
- Continuous reports of the acquisition strategy and status.
- Regular (quarterly) financial balances to the KIT project management.
- A resource-loaded project plan maintained and updated on a server for continuous access.
- Milestone plan with milestone tracking.
- Regular meetings with the PPQ (*Projekt-, Prozess- und Qualitätsmanagement*) department of KIT.

V. CONCLUSION AND OUTLOOK

The KATRIN experiment provides the unique chance of exploring the tritium β-decay spectrum in a wide energy range with unprecedented sensitivity. Such measurement opens up the possibility to search for physics beyond the Standard Model not accessible elsewhere.

A novel detector and read-out system is necessary to extend the measurement interval. Over the past years we succeeded in developing a full design of the system, which entails a large-area, low-noise SDD focal plane array, ASIC-based read-out electronics, and a high-performance DAQ system.

The system is subdivided in modules each comprising 166 detector pixels. In the first stage of the phase-0 integration, we successfully demonstrated the operation of a single module in the MAC-E filter environment of the monitoring spectrometer of the KATRIN experiment. The measurements show that the excellent energy resolution, pixel homogeneity, vacuum and magnetic field compatibility could be reached as planned. Based on these first results, phase-1, consisting of 9 modules is currently under construction. Its size is suitable to be integrated

in the KATRIN beam line without significant modification of the KATRIN detector chamber. The integration is planned for 2024. The final stage of the experiment is the extension to 21 modules (phase-2), with the goal to reach the ultimate sensitivity to sterile neutrinos at a mixing angle of $10^{-}6$ and masses up to about 15 keV.

ACKNOWLEDGEMENTS

We acknowledge the support of Helmholtz Association (HGF), Ministry for Education and Research BMBF (05A20PMA, 05A20PX3, 05A20VK3), Helmholtz Alliance for Astroparticle Physics (HAP), the doctoral school KSETA at KIT, and Helmholtz Young Investigator Group (VH-NG-1055) in Germany; Ministry of Education, Youth and Sport (CANAM-LM2015056, LTT19005) in the Czech Republic; and the Department of Energy through grants DE-FG02-97ER41020, DE-FG02-94ER40818, DE-SC0004036, DE-FG02-97ER41033, DE-FG02-97ER41041, DE-AC02-05CH11231, and DE-SC0011091 in the United States. This project has received funding from the European Research Council (ERC) under the European Unionís Horizon 2020 research and innovation programme (grant agreement No. 852845).

[1] M. Aker *et al.* (KATRIN Collaboration), arXiv, e-print: 2105.08533 (2021).
[2] S. Dodelson and L. M. Widrow, Phys. Rev. Lett. **72**, 17 (1994).
[3] L. Canetti, M. Drewes, and M. Shaposhnikov, Phys. Rev. Lett. **110**, 061801 (2013).
[4] X. Shi and G. M. Fuller, Phys. Rev. Lett. **82**, 2832 (1999).
[5] Q. Zhu, F. Marinacci, M. Maji, Y. Li, V. Springel, and L. Hernquist, Mon. Not. Roy. Astron. Soc. **458**, 1559 (2016), arXiv:1506.05537 [astro-ph.CO].
[6] R. Murgia, A. Merle, M. Viel, M. Totzauer, and A. Schneider, Journal of Cosmology and Astroparticle Physics **2017** (11), 046.
[7] D. V. Otokar Dragoun, Open Physics Journal **3**, 73 (2016).
[8] R. Shrock, Physics Letters B **96**, 159 (1980).
[9] H. de Vega, O. Moreno, E. M. de Guerra, M. R. Medrano, and N. Sánchez, Nuclear Physics B **866**, 177 (2013).
[10] S. Mertens, T. Lasserre, S. Groh, *et al.*, J. Cosmol. Astropart. Phys. **2015** (02), 020.
[11] C. R. Watson, Z. Li, and N. K. Polley, Journal of Cosmology and Astroparticle Physics **2012** (03), 018.
[12] A. Boyarsky, D. Iakubovskyi, O. Ruchayskiy, and V. Savchenko, Monthly Notices of the Royal Astronomical Society **387**, 1361 (2008).
[13] R. Adhikari *et al.*, Journal of Cosmology and Astroparticle Physics **2017** (01), 025.
[14] C. Benso, V. Brdar, M. Lindner, and W. Rodejohann, Phys. Rev. D **100**, 115035 (2019), arXiv:1911.00328 [hep-ph].
[15] G. Arcadi, J. Heeck, F. Heizmann, S. Mertens, F. S. Queiroz, W. Rodejohann, M. Slezák, and K. Valerius, JHEP **01**, 206, arXiv:1811.03530 [hep-ph].
[16] P. O. Ludl and W. Rodejohann, JHEP **06**, 040, arXiv:1603.08690 [hep-ph].
[17] W. Rodejohann and H. Zhang, Phys. Lett. B **737**, 81 (2014), arXiv:1407.2739 [hep-ph].
[18] J. Barry, J. Heeck, and W. Rodejohann, JHEP **07**, 081, arXiv:1404.5955 [hep-ph].
[19] M. Korzeczek, *Sterile neutrino search with KATRIN - modeling and design-criteria of a novel detector system*, Ph.D. thesis, Karlsruher Institut für Technologie (KIT) (2020), 51.03.02; LK 01.
[20] S. Mertens, A. Alborini, K. Altenmüller, T. Bode, L. Bombelli, T. Brunst, M. Carminati, D. Fink, C. Fiorini, T. Houdy, A. Huber, M. Korzeczek, T. Lasserre, P. Lechner, M. Manotti, I. Peric, D. C. Radford, D. Siegmann, M. Slezák, K. Valerius, J. Wolf, and S. Wüstling, Journal of Physics G: Nuclear and Particle Physics **46**, 065203 (2019).
[21] K. Dolde, S. Mertens, D. Radford, T. Bode, A. Huber, M. Korzeczek, T. Lasserre, and M. Slezak, Nucl. Instrum. Meth. A **848**, 127 (2017), arXiv:1608.03158 [physics.ins-det].
[22] A. Huber, *Analysis of first KATRIN data and searches for keV-scale sterile neutrinos*, Ph.D. thesis, Karlsruher Institut für Technologie (KIT) (2021), 51.03.01; LK 01.
[23] E. Förstner, Optimization of the KATRIN rear wall for a keV-scale sterile neutrino search (2017).
[24] N. M. N. Steinbrink, J. D. Behrens, S. Mertens, P. C. O. Ranitzsch, and C. Weinheimer, Eur. Phys. J. C **78**, 212 (2018), arXiv:1710.04939 [physics.ins-det].
[25] S. Mertens *et al.*, Journal of Physics G: Nuclear and Particle Physics (2020).
[26] M. Gugiatti, M. Biassoni, M. Carminati, O. Cremonesi, C. Fiorini, P. King, P. Lechner, S. Mertens, L. Pagnanini, M. Pavan, *et al.*, Nuclear Instruments and Methods in Physics Research Section A: Accelerators, Spectrometers, Detectors and Associated Equipment **979**, 164474 (2020).
[27] M. Arenz *et al.*, Journal of Instrumentation **11** (04), P04011.
[28] P. King, M. Gugiatti, M. Carminati, L. Buonanno, G. Borghi, G. Pepponi, P. Lechner, D. Siegmann, K. Urban, T. Houdy, *et al.*, Journal of Instrumentation **16** (07), T07007.